In conclusion, by exploring the short-pulse limit of superradiant Rayleigh scattering, we have observed a previously unknown phenomenon in the scattering of a single laser beam by atoms: self-stimulated Kapitza-Dirac diffraction. The symmetry of the diffraction pattern implies a reduced gain for both atom and light amplification at early times. This realizes a novel regime of superradiance in which the atomic system has three almost equally spaced levels with all of the initial population in the middle one. This system has allowed us to illustrate important concepts of stimulation and superradiance. In the Dicke picture, all photons are emitted spontaneously and simply leave the system. However, we directly observed stimulation by and absorption of these photons in the form of Kapitza-Dirac scattering, and therefore the Dicke picture is incomplete for the short-pulse regime. None of the theoretical descriptions of superradiance in Bose-Einstein condensate (*5*, *7*–*12*) included transitions to momentum states that appear as negative orders in Kapitza-Dirac scattering.

Extrapolating our observations of Kapitza-Dirac scattering to longer pulses establishes the equivalence of self-stimulated Bragg diffraction and matter-wave amplification. There is a widespread opinion that bosonic stimulation is a purely quantum-statistical effect based on symmetry, whereas (*3*, *4*) showed that bosonically enhanced scattering can always be traced back to enhanced fluctuations. Here we have directly shown how photons mediate an effective interaction between the atoms that, after elimination of the photon field, results in bosonic stimulation of atoms. However, at early times, the "stimulating effect" of the population in mode q interferes destructively with the effect of atoms in mode $-q$ and the basic concept of bosonic stimulation by atoms fails, whereas a simple picture of optical stimulation provides the correct answer (*20*).

References and Notes

1. R. H. Dicke, *Phys. Rev.* **93**, 99 (1954).
2. M. Gross, S. Haroche, *Phys. Rep.* **93**, 301 (1982).
3. W. Ketterle, S. Inouye, *Phys. Rev. Lett.* **86**, 4203 (2001).
4. M. G. Moore, P. Meystre, *Phys. Rev. Lett.* **86**, 4199 (2001).
5. S. Inouye *et al.*, *Nature* **402**, 641 (1999).
6. M. Kozuma *et al.*, *Science* **286**, 2309 (1999).
7. W. Ketterle, S. Inouye, in *Bose-Einstein Condensates and Atom Lasers*, A. Aspect, J. Dalibard, Eds., vol. IV of *Comptes Rendus de l'Académie des Sciences Paris* (Elsevier, Paris, 2001), pp. 339–380.
8. S. Inouye *et al.*, *Science* **285**, 571 (1999).
9. M. G. Moore, P. Meystre, *Phys. Rev. Lett.* **83**, 5202 (1999).
10. Ö. E. Müstecaplioglu, L. You, *Phys. Rev. A* **62**, 063615 (2000).
11. N. Piovella, R. Bonifacio, B. W. J. McNeil, G. R. M. Robb, *Opt. Commun.* **187**, 165 (2001).
12. E. D. Trifonov, *J. Exp. Theor. Phys.* **93**, 969 (2001) [translation from E. D. Trifonov, *Zh. Eksp. Teor. Fiz.* **120**, 1117 (2001)].
13. P. J. Martin, B. G. Oldaker, A. H. Miklich, D. E. Pritchard, *Phys. Rev. Lett.* **60**, 515 (1988).
14. M. Kozuma *et al.*, *Phys. Rev. Lett.* **82**, 871 (1999).
15. P. L. Gould, G. A. Ruff, D. E. Pritchard, *Phys. Rev. Lett.* **56**, 827 (1986).
16. Y. B. Ovchinnikov *et al.*, *Phys. Rev. Lett.* **83**, 284 (1999).
17. For the 30-ms time of flight, the condensate expands by only 10% in the axial direction, as compared to more than a factor of 15 in the radial direction.
18. The fractional solid angle subtended by the condensate is $\Omega \sim (d^2/L^2)/4\pi$, where d is its diameter and L its length. The contribution of spontaneous Rayleigh scattering to the endfire mode intensity thus is on the order of $\Omega \times (N\Gamma_{sc}\hbar\omega) \times 1/d^2 = 2.5 \times 10^{-3}$ m W cm^{-2}.
19. J. Stenger *et al.*, *Phys. Rev. Lett.* **82**, 4569 (1999).
20. We would like to thank G. Campbell, A. Leanhardt, and J. Steinhauer for a critical reading of the manuscript and P. Meystre and S. Inouye for discussions. This work was supported by NSF.

7 February 2003; accepted 18 March 2003
Published online 27 March 2003;
10.1126/science.1083171
Include this information when citing this paper.

Mantle Fault Zone Beneath Kilauea Volcano, Hawaii

Cecily J. Wolfe,[1]* Paul G. Okubo,[2] Peter M. Shearer[3]

Relocations and focal mechanism analyses of deep earthquakes (≥13 kilometers) at Kilauea volcano demonstrate that seismicity is focused on an active fault zone at 30-kilometer depth, with seaward slip on a low-angle plane, and other smaller, distinct fault zones. The earthquakes we have analyzed predominantly reflect tectonic faulting in the brittle lithosphere rather than magma movement associated with volcanic activity. The tectonic earthquakes may be induced on preexisting faults by stresses of magmatic origin, although background stresses from volcano loading and lithospheric flexure may also contribute.

Earthquake characteristics at the active Kilauea volcano have long been used to construct models of this shield volcano and to constrain the structure of its magmatic system (*1*–*4*). Based on hypocenters in the catalog of the U.S. Geological Survey Hawaiian Volcano Observatory (HVO) seismic network, it has been suggested that the earthquakes at Kilauea outline a pipe-like magma conduit that extends through the lithosphere to depths as great as 60 km (*1*–*4*), thereby delineating the magma pathway from its source to the surface. However, the accuracy of routinely determined hypocenters is limited by factors including the network geometry, the available arrival time picks, picking errors, and the presence of three-dimensional velocity heterogeneity. Thus, relocations of earthquakes, using relative location methods, which reduce the effects of velocity heterogeneity, combined with precise cross-correlation measurements, have produced more accurate locations (*5*–*11*) and delineated fault structures. Here, we present relocations of deep earthquakes, focusing on distinguishing magmatic versus tectonic events to understand how the growing volcano affects the crust and upper mantle.

[1]Hawaii Institute of Geophysics and Planetology, University of Hawaii at Manoa, Honolulu, HI 96822, USA. [2]Hawaiian Volcano Observatory, U.S. Geological Survey, Hawaii National Park, HI 96718, USA. [3]Scripps Institution of Oceanography, University of California at San Diego, La Jolla, CA 92093–0225, USA.

*To whom correspondence should be addressed. E-mail: wolfe@hawaii.edu

Our data consist of waveforms from 1988 to 1998 in the catalog of routinely located deep earthquakes recorded by the HVO seismic network, amounting to 14,604 events spread across and around Hawaii. The voluminous Pu′u ′O′o-Kupaianaha eruption of Kilauea, which began in 1983 and still continues, was occurring throughout the study period. The seismic events at Kilauea can be classified into three types, (i) high-frequency earthquakes that indicate shear faulting, and (ii) long-period (LP) earthquakes and (iii) tremor (*12*, *13*) that likely reflect resonance in fluid-filled conduits. The data set contains 2376 LP events, with 90% above 20-km depth, and 135 tremor events, with 90% below 30-km depth (*14*).

Precise arrival time differences for earthquake pairs were obtained using waveform cross correlation with parameters appropriate for high-frequency earthquakes (*15*), and these data were able to relocate 7034 hypocenters, or 48% of the analyzed events. This calculation is a minimum estimate of the number of similar events, because pairs will not correlate highly if the signal-to-noise ratio is low: small magnitude events that are displaced far from stations, such as small, deeper earthquakes, are more difficult to constrain. Families of highly correlated earthquakes occur when there are closely spaced clusters with similar focal mechanisms, as at fault zones. Hence, our relocated clusters identify fault zones in the lithosphere beneath Hawaii.

The subset of 2522 earthquakes relocated in the vicinity of Kilauea is shown in Figs. 1 and 2, and fig. S1 displays the total set of 7034

relocated earthquakes. One of the main features of the relocated seismicity at Kilauea is that a cluster of earthquakes near 30-km depth (Fig. 2B) collapses to reveal a horizontally aligned fault zone (Fig. 2A), with 1030 of the relocated earthquakes at depths of 26 to 32 km (fig. S2). The distribution of relocated earthquakes also reveals several small, spatially distinct and unconnected fault zones, including ones that extend deeper offshore. There are only 92 earthquakes relocated between 16- and 24-km depth. Below 16-km depth the events that we relocated do not suggest a magma conduit through the lithosphere (Fig. 2A), and such a feature also is not obvious in the patterns of the unrelocated earthquakes (Fig. 2C).

Although 632 earthquakes were relocated at depths shallower than 16 km (Fig. 2A), 2163 earthquakes located 13 to 20 km beneath Kilauea did not correlate (Figs. 1C and 2C), and 1731 of these are LP events that may reflect magmatic processes. In a separate analysis using different parameters (*16*), we were able to correlate and relocate 1256 LP events at Kilauea (fig. S3). In these relocations, a cylindrical cloud of seismicity at 13- to 20-km depth collapses to a more localized feature at 14- to 16-km depth. Based on constraints from seismic and gravity data (*17*), these relocated shallower LP earthquakes may occur just above the base of the crust at Kilauea and could plausibly reflect a magma conduit in the crust.

The presence of a tectonic fault zone near 30-km depth is supported by the mechanisms of the earthquakes. In 1994, a large teleseismically recorded earthquake, with body-wave magnitude m_b 5.3 reported by the National Earthquake Information Center, occurred near 30-km depth at Kilauea (Fig. 2D), and the best double-couple mechanism was determined from the Harvard centroid moment tensor catalog (*18*) (Fig. 1E). For larger events ($\sim m_L > 1.5$), catalog travel time picks and phase polarities were available from 1974 to 2000. Composite mechanisms (*19*) for earthquakes with catalog locations near the 30-km deep cluster (Fig. 2) indicate that the dominant style of faulting is equivalent to the mechanism of the 1994 m_b 5.3 earthquake (Fig. 1E and fig. S4). The pattern of aftershocks of the 1994 m_b 5.3 earthquake is consistent with rupture being on the low-angle fault plane with seaward slip (*20*) rather than on the northeast oriented vertical plane with oblique dip-slip motion.

Catalog locations and magnitudes (Fig. 2D) further indicate the existence of a long-lived tectonic fault zone near 30-km depth (*21*) that has been active for at least about 40 years. Between depths of 20 and 40 km, the available HVO catalog of larger ($\sim m_L \geq 1.5$) earthquakes from October 1959 through 2000 demonstrates that the region (Fig. 1) regularly experiences $m_L \geq 4$ earthquakes, with 73 occurring in this time period. Moreover, of the 1011 $m_L \geq 3$ Hawaiian earthquakes in this depth and time interval, 42% occur in the area around Kilauea, making it by far the most seismically active region at depths of 20 to 40 km. Plots of the cumulative number of events versus time reveal that this region generally experiences a steady rate of earthquakes rather than swarm characteristics (*22*).

The association of this highly active seismic zone with the frequently erupting Kilauea volcano implies that the tectonic faulting is related to stresses of magmatic origin, although the background stresses from volcano loading and flexure may help bring faults close to failure. The mechanism of the faulting at 30-km depth, seaward slip on a low-angle plane, is similar to the mechanisms of earthquakes on a shallow crustal detachment believed to exist at the interface between Kilauea volcano and the preexisting oceanic crust (*6*, *23*). It has been proposed that movement on this shallow detachment is driven by intrusion of magma into a deep dikelike body (*24*, *25*). The magma pathways in the mantle beneath Kilauea may analogously create stresses that, in combination with the ambient stresses from volcano loading and flexure, produce deep earthquakes on preexisting faults.

Our analyses did not find correlated deep clusters of high-frequency earthquakes at

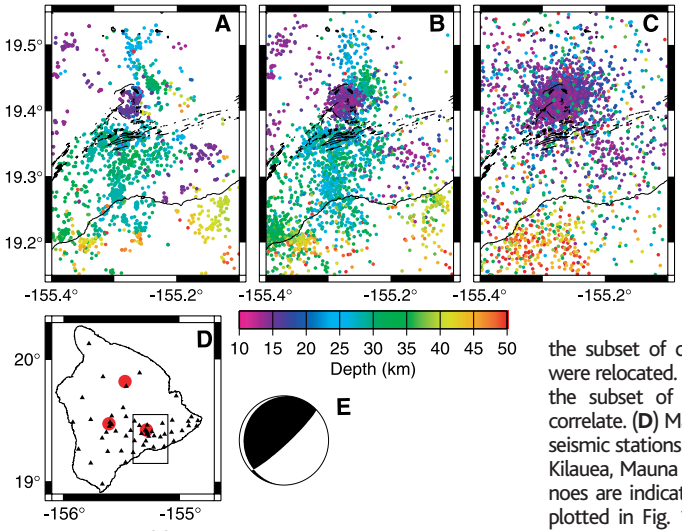

Fig. 1. Map view of earthquakes (1988–1998) at Kilauea with features of Kilauea caldera drawn as lines. Earthquake locations are plotted as circles, with color indicating hypocentral depth. (**A**) Relocated hypocenters derived using cross-correlation arrival time differences. (**B**) Original catalog hypocenters for the subset of correlated earthquakes that were relocated. (**C**) Catalog hypocenters for the subset of earthquakes that did not correlate. (**D**) Map of the HVO short-period seismic stations (triangles). The locations of Kilauea, Mauna Loa, and Mauna Kea volcanoes are indicated (red circles). The region plotted in Fig. 1, A to C, is denoted by a rectangular box. (**E**) Best double-couple focal mechanism of a 1994 m_b 5.3 earthquake near 30-km depth from the Harvard centroid moment tensor catalog (*18*).

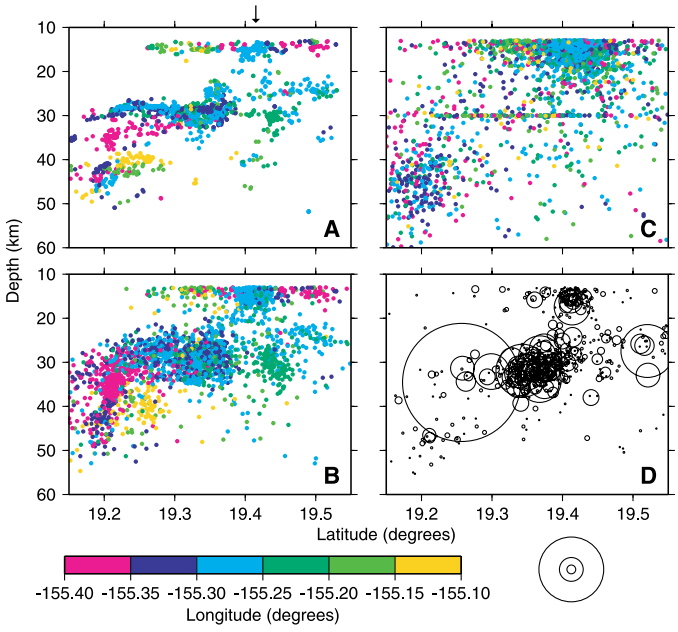

Fig. 2. Vertical cross sections of the region in Fig. 1. Earthquake locations are plotted as circles, with color indicating hypocenter longitude. (**A**) Relocated hypocenters derived using cross-correlation arrival time differences. The location of Kilauea caldera is indicated by a vertical arrow. (**B**) Original catalog hypocenters for the subset of correlated earthquakes that were relocated. (**C**) Catalog hypocenters for the subset of earthquakes that did not correlate. Note that the line of horizontal earthquakes in the catalog locations of Fig. 2C are poorly constrained events whose depths were fixed to 30 km. (**D**) Catalog hypocenters for earthquakes ($m_L \geq 3.0$) from October 1959 through December 2000. The radius of the circle is a function of m_L, with the radii for m_L 4.0, 4.5, and 5.0 given by concentric circles plotted below the panel.

Mauna Loa volcano, which was not erupting during the time period 1988–1998. However, our analyses relocated many clusters of earthquakes parallel to the southeast coast of Hawaii at depths of 25 to 50 km (fig. S1), indicating the existence of several tectonic fault zones in the mantle throughout this region. Earthquakes at these fault zones, which occur seaward of Kilauea and Mauna Loa volcanoes, may similarly be caused by broader melt movements and the effects of volcano loading and flexure.

References and Notes

1. J. P. Eaton, K. J. Murata, *Science* **132**, 925 (1960).
2. F. W. Klein, R. Y. Koyanagi, J. S. Nakata, W. R. Tanigawa, *U.S. Geol. Surv. Prof. Paper* **1350**, 1019 (1987).
3. R. I. Tilling, J. J. Dvorak, *Nature* **363**, 125 (1993).
4. M. P. Ryan, *J. Geophys. Res.* **93**, 4213 (1988).
5. G. Poupinet, W. L. Ellsworth, J. Frechet, *J. Geophys. Res.* **89**, 5719 (1984).
6. J.-L. Got, J. Frechet, F. W. Klein, *J. Geophys. Res.* **99**, 15375 (1994).
7. R. M. Nadeau, W. Foxall, T. V. McEvilly, *Science* **267**, 503 (1995).
8. D. Gillard, A. M. Rubin, P. Okubu, *Nature* **384**, 343 (1996).
9. P. M. Shearer, *J. Geophys. Res.* **102**, 8269 (1997).
10. A. M. Rubin, D. Gillard, J.-L. Got, *Nature* **400**, 635 (1999).
11. F. Waldhauser, W. L. Ellsworth, *Bull. Seismol. Soc. Am.* **90**, 1353 (2000).
12. R. Y. Koyanagi, B. Chouet, K. Aki, *U.S. Geol. Surv. Prof. Paper* **1350**, 1221 (1987).
13. B. A. Chouet, *Nature* **380**, 309 (1996).
14. The subjective identification of LP events and tremor is made at HVO as part of their operations. The catalog we used only includes located LP events and tremor and does not include events that could not be picked and located.
15. Materials and methods are available as supporting material on *Science* Online.
16. For the separate analysis of LP events, we used 21.5-s time windows, bandpass filtered the seismic data 1 to 15 Hz, and took a correlation threshold of 0.4. Note that of the 632 relocated events above 16-km depth in Figs. 1A and 2A (*15*), 297 are high-frequency earthquakes and 335 are LP events.
17. D. P. Hill, J. J. Zucca, *U.S. Geol. Surv. Prof. Paper* **1350**, 903 (1987).
18. A. M. Dziewonski, G. Ekstrom, M. P. Salganik, *Phys. Earth Planet. Inter.* **86**, 253 (1994).
19. Materials and methods are available as supporting material on *Science* Online.
20. The aftershocks of the 1994 m_b 5.3 earthquake make up a large proportion of the seismicity at 30-km depth between latitudes of 19.2° to 19.3° at –155.3° longitude, forming a north-south–oriented line of epicenters.
21. The relocation of earthquakes from 1974 to 2000 using difference pairs from the catalog travel time data yields images consistent with Figs. 1 and 2. However, as expected, given the larger errors in hand-picked arrival times, the patterns are not as sharply defined as when using arrival time differences from cross correlation.
22. Seismic swarms are episodes when the rates of earthquakes are highly increased without the presence of a large magnitude mainshock. Although the time interval and spatial region we examined did not display swarms, occasional earthquake swarms at depths of 45 to 65 km were observed from the early 1950s until the fall of 1960 (*26*).
23. The mechanisms of shallow earthquakes along the south flank of Hawaii in the Harvard centroid moment tensor catalog (1976–2002) (*18*) generally show seaward slip on low-angle fault planes.
24. P. T. Delaney, R. S. Fiske, A. Miklius, A. T. Okamura, M. K. Sako, *Science* **247**, 1311 (1990).
25. S. Owen *et al.*, *Science* **267**, 1328 (1995).
26. J. P. Eaton, D. H. Richter, H. Krivoy, *U.S. Geol. Surv. Prof. Paper* **1350**, 1307 (1987).

27. This research was supported by NSF under grant EAR-0106357. We thank J. Battaglia, B. Brooks, G. Ekström, J.-L. Got, F. Klein, S. Koyanagi, M. Nettles, G. Pavlis, A. Rubin, and S. Solomon for thoughtful comments. This is School of Ocean and Earth Science and Technology (SOEST) contribution number 6219 and Hawaii Institute of Geophysics and Planetology (HIGP) contribution number 1272.

Supporting Online Material

www.sciencemag.org/cgi/content/full/300/5618/478/DC1
Materials and Methods
Figs. S1 to S4
Table S1
References and Notes

9 January 2003; accepted 13 March 2003

A 23,000-Year Record of Surface Water pH and PCO_2 in the Western Equatorial Pacific Ocean

M. R. Palmer[1]* and P. N. Pearson[2]

The oceans play a major role in defining atmospheric carbon dioxide (CO_2) levels, and although the geographical distribution of CO_2 uptake and release in the modern ocean is understood, little is known about past distributions. Boron isotope studies of planktonic foraminifera from the western equatorial Pacific show that this area was a strong source of CO_2 to the atmosphere between approximately 13,800 and 15,600 years ago. This observation is most compatible with increased frequency of La Niña conditions during this interval. Hence, increased upwelling in the eastern equatorial Pacific may have played an important role in the rise in atmospheric CO_2 during the last deglaciation.

It is generally accepted that the oceans played a major role in controlling changes in the CO_2 content of the atmosphere over glacial-interglacial time scales (*1*). Although there is uncertainty regarding the exact processes (*2*), they must have involved changes in the areas of the surface oceans that are supersaturated or undersaturated with CO_2 with respect to the atmosphere and/or changes in the magnitude of the difference between the partial pressure of CO_2 (PCO_2) of surface waters and the atmosphere. Hence, an important constraint on the mechanism of glacial-interglacial changes in atmospheric CO_2 would be provided by comparing the PCO_2 of surface waters of the glacial ocean with those during deglaciation and today. Oceanographic studies have resulted in maps delineating the PCO_2 in surface waters of the modern ocean (*3*), and we show here that boron isotope ($\delta^{11}B$) analyses of planktonic foraminifera offer the opportunity to provide similar information about the past.

Experimental studies have shown that the planktonic foraminifer *Globigerinoides sacculifer* faithfully records the $\delta^{11}B$ of dissolved $B(OH)_4^-$ in the seawater from which the foraminifer grew its shell (*4*), and that this is directly related to the pH of the seawater. By using the pH of the seawater and either the alkalinity or the dissolved inorganic carbon concentrations, the PCO_2 of the waters can be calculated (*5*).

The equatorial Pacific is the site of the greatest evasion of CO_2 (0.8 to 1.0 Pg C $year^{-1}$) from the modern oceans (*3*), and may thus have played a role in glacial-interglacial changes in atmospheric PCO_2. In this study, we determined the $\delta^{11}B$ of 31 handpicked samples of ~50 *G. sacculifer* (500 to 600 μm) from box core ERDC-92 that was raised from the western equatorial Pacific (2°13.5′S, 156°59.9′E; 1598 m) (*6*). The samples range from 0.4 to 23.2 thousand years ago (ka) (*7*, *8*) and cover the period from the last glacial maximum to almost the present day. $\delta^{11}B$ values were determined at Southampton using analytical techniques that are described in (*9*) and the data are listed in Table 1. Carbon and oxygen isotopes were measured at Cardiff using standard techniques. Because boron isotope fractionation and the dissociation of boric acid and carbonate species are temperature dependent, the Mg/Ca ratios of the selected samples were measured and the temperatures were calculated using the Mg/Ca-temperature relationship of Dekens *et al.* (*10*) (and by interpolating for intervening samples).

Figure 1 illustrates the variations in $\delta^{11}B$ (Fig. 1A), calculated pH (Fig. 1B), and surface water PCO_2 values (Fig. 1C). Also included are atmospheric PCO_2 levels (from the Taylor Dome ice core record (*11*, *12*) (Fig.

[1]School of Ocean and Earth Sciences, Southampton Oceanography Centre, European Way, Southampton SO14 3ZH, UK. [2]Department of Earth Sciences, Cardiff University, Main Building, Post Office Box 914, Cardiff CF10 3YE, UK.

*To whom correspondence should be addressed. E-mail: pmrp@soc.soton.ac.uk